Background Pressure Effect on Electron Acceleration from Ultra-Intense Laser-Matter Interactions

Undergraduate Research Thesis

Presented in Partial Fulfillment of the Requirements for graduation "with Honors Research Distinction in Physics" in the undergraduate colleges of The Ohio State University

by
Manh Le

The Ohio State University
April 2018

Advisor: Professor Chris Orban and Professor Enam Chowdhury

Abstract

We present two-dimensional particle-in-cell (PIC) simulations that investigate the role of background pressure on the acceleration of electrons from ultra intense laser interaction at normal incidence with liquid density ethylene glycol targets. The interaction was simulated at ten different pressures varying from 7.8 mTorr to 26 Torr. We calculated conversion efficiencies from the simulation results and plotted the efficiencies with respect to the background pressure. The results revealed that the laser to electron conversion efficiency for electron energies greater than 100 keV remained around 0.35% from 7.8 mTorr to 1.2 Torr and increased exponentially from 1.2 Torr onward to about 2.2% at 90 Torr. Increasing the background pressure clearly has a dramatic effect on the acceleration of electrons from the target. We explain how electrostatic effects, in particular the neutralization of the target by the background plasma, allows electrons to escape more easily and that this effect is strengthened with higher densities. This work could facilitate the design of future experiments in increasing laser to energetic electron conversion efficiency and generating substantial bursts of electrons with relativistic energies. Furthermore, understanding electron dynamics will provide deeper insight into the effect on ion acceleration.

1 Background

High-energy accelerated particles are particularly useful for scientific research and engineering. Beams of energetic particles, for example, have applications in medicine such as cancer radiotherapy and as sources for diagnostic techniques.[1] For example, high-energy neutrons can be generated from accelerated charged particles, and can be used to perform nondestructive evaluation of materials. However, accelerating high-energy charged particles for use in hospitals, for example, currently requires large facilities. Likewise, nuclear reactors are often used as the typical high-energy neutron sources, which have monetary, spatial, and security constraints. However, ultra-intense short

pulse lasers are also capable of accelerating beams of high-energy particles including ions through a variety of mechanisms resulting from laser-matter interactions, a couple of which are radiation pressure acceleration (RPA) and target-normal sheath acceleration (TNSA).[2] Additionally, short pulse laser tabletop setups have an advantage over current approaches in that they can serve as compact alternatives to current facilities.

1.1 Experiment at AFRL

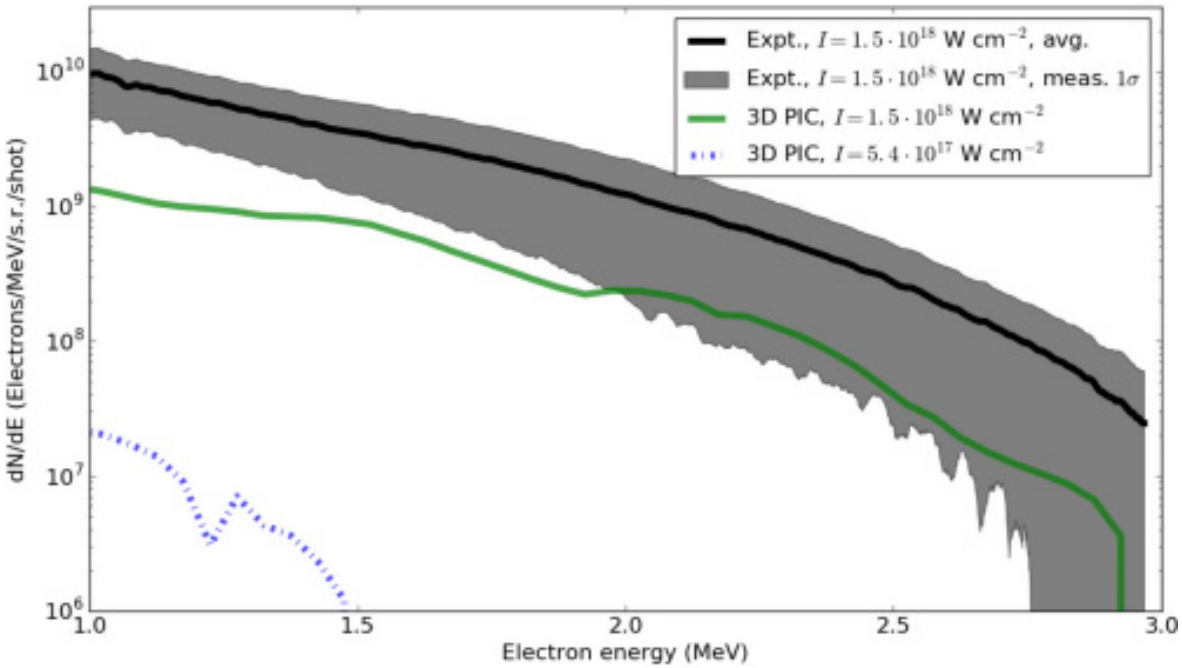

Figure 1: Energy characterization of electrons accelerated opposite the laser propagation direction under an ambient pressure in the target chamber of 20 Torr. The black line represents the mean of 50 energy spectra and the gray area represents the standard deviation of the measured spectra. The green and purple lines are particle-in-cell (PIC) simulation results.[3]

The experiment at the Extreme Light Lab at the Air Force Research Laboratory investigated laser-ion acceleration using a short pulse, ultra-intense laser in conjunction with a liquid sheet target. These experiments accelerated charged particles to relativistic energies (MeV). Typical short pulse laser experiments involving TNSA use a solid target and cannot achieve a high repetition rate. The

Red Dragon laser at AFRL, however, is capable of generating a ultra-intense laser (10^{18} W/cm^2) with a very high repetition rate of 1 kHz and uses a liquid sheet with a thickness of about half of a micron as the target.[1] This thin liquid sheet is formed using two colliding jets.[1] Liquid targets have a similar density to solids and regenerate quickly between shots whereas a solid target would be depleted and thus be incapable of supporting such a high repetition rate. Additionally, laser pulse interaction with a solid target may produce solid debris that may damage optics. The advantage of a high repetition rate is that a lot of data can be collected quickly compared to other setups that may only perform a few shots per day; a high repetition rate also allows more particles to be accelerated over a given amount of time.

Initial experiments with the AFRL setup used liquid water targets and were performed at an ambient pressure of 20 Torr [4, 3]. This pressure is about as low as can be achieved with water targets due to the high partial pressure of water. Liquid water is unable to remain in liquid phase at a lower ambient pressure; as a result, it boils off and causes the water jets to freeze via evaporative cooling.[3] These experiments revealed a higher laser-to-electron conversion efficiency than expected; more of the laser energy went into accelerating electrons compared to short pulse experiments with solid targets in vacuum as shown in Figure 1.[4, 3] The experimentalists later discovered that there was essentially no ion acceleration at these pressures. Experiments at a lower pressure than 20 Torr showed ion acceleration but a lower laser-to-electron conversion efficiency. The difference was attributed to the ambient, or background pressure.

1.2 Target-Normal Sheath Acceleration

Short pulse lasers are capable of accelerating charged particles to relativistic speeds (near the speed of light) through a mechanism known as target-normal sheath acceleration, or TNSA.[2] Target-

normal sheath acceleration is an effect created by the laser pulse's interaction with the plasma.[1, 2] The pre-pulse, which is a secondary pulse that is often orders of magnitude lower in intensity than the main pulse, ionizes the target, ripping electrons from their atoms and creating a plasma, a gas of charged particles. The laser pulse accelerates some of the electrons (ions, being so massive compared to electrons, are not moved significantly on the timescale of the pulse) away from the target creating a positive charge on the target.[1, 2] This draws the accelerated electrons back toward the target. Some of the accelerated electrons are turned around and do not escape the target. These electrons are still highly energetic and so recirculate as a cloud, or sheath of negative charge outside the target. This cloud creates an electrostatic potential gradient that draws ions out of the target and accelerates them away from the target as shown in Figure 2.[1, 2]

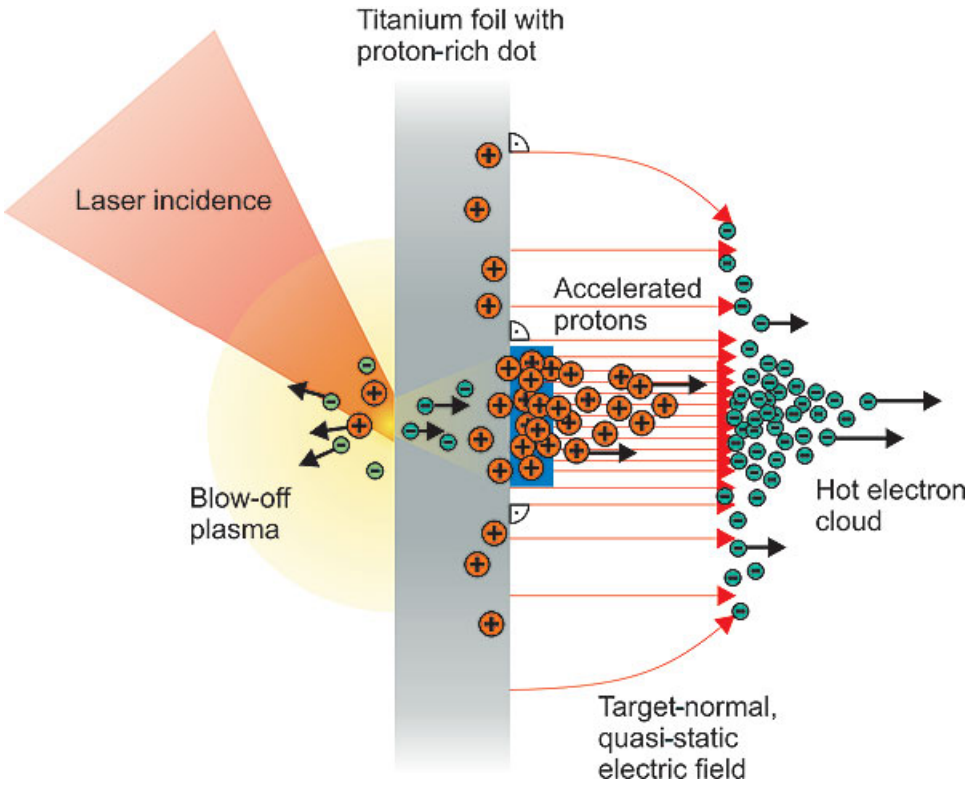

Figure 2: Visual overview of the mechanism of target-normal sheath acceleration. The laser accelerates electrons off the target, charging it up and creating an electron sheath around it. Ions are then accelerated by the electron sheath.[5]

2 Theory

Our hypothesis is that the high background pressure minimizes electrostatic effects that would occur in vacuum and thus facilitates the acceleration of electrons from the target. In a vacuum, when the laser pulse accelerates electrons from the target, the deficit of electrons charges up the target and the now charged target pulls some of the electrons back. The presence of a background plasma mitigates this. The background plasma acts as a reservoir of electrons to neutralize the target, so the charged target pulls in electrons from its surroundings instead of the accelerated electrons. Fewer electrons are turned around, and more electrons escape.

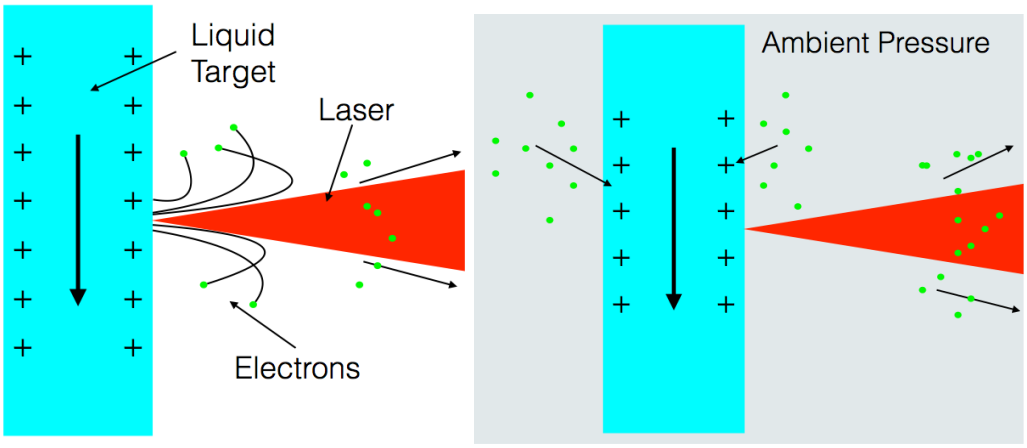

(a) Vacuum (b) Background Pressure

Figure 3: Illustration of hypothesis. (a) In vacuum, the electrons are being turned around by the charged up target. (b) The denser background plasma mitigates this by acting as a reservoir of electrons to neutralize the charge.

2.1 Capacitor Model

In Link *et al*, the effect of the target charging up on electron acceleration was modeled by treating the system as a capacitor system as shown.[6] According to Link *et al*, this simple model of the target charging up similar to a capacitor was in strong agreement with the predictions of

simulations despite not containing any physics related to scattering, electric or magnetic fields, or electron-electron interactions.[6] The target acts as one side of the capacitor with the other side of the capacitor out at infinity. For a sufficiently large charge, the effect of accelerated electrons on the potential is minimal. However, for small charges, the accelerated electrons substantially change the charge on the target and thus the potential seen. According to the capacitor model, these electrostatic effects heavily influence the energy spectra of the emitted electrons.[6]

2.2 Derivation

In the case of a background pressure, however, the capacitor is essentially being discharged as ambient surrounding electrons move in to neutralize the positive charge of the target. Where, in a vacuum, the target would charge up like a capacitor and create the potential that escaping electrons must overcome, the addition of a background pressure essentially allows for the capacitor to discharge. The typical scenario for the discharging of a capacitor would the resistor-capacitor (RC) circuit with

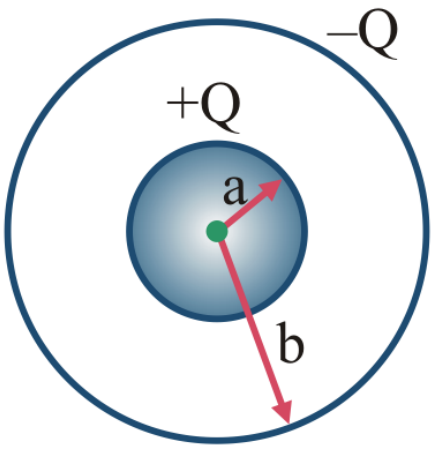

Figure 4: Illustration of a spherical capacitor which serves as a simplified model for the target during the electron acceleration stage of TNSA.

the following differential equation describing its behavior.

$$\frac{Q}{C} = -R\frac{dQ}{dt}$$

However, this model assumes that the electrons are moving about essentially randomly due to thermal contributions and that there is some sort of resistance. In the Drude model, the drift velocity would be directly proportional to **E**, the electric field, and by extension the charge Q. In this case on the other hand, the electrostatic fields on this scale are sufficiently strong that the electrons are free-flowing and moving in the same direction; the electrostatic contribution is much larger than thermal contributions. Additionally, the electrons are coming in from the air and have no constraints to their motion as in a wire. Therefore, the typical RC model would not be suitable to model this scenario. Instead, the discharge should be modeled as a free flow of electrons into the target. The differential equation to model this scenario is:

$$\frac{-dQ}{dt} = -I = -e * n_e * v_d * A \tag{1}$$

In the experiment, the background electron density is known from measuring the air pressure in the chamber. For better comparison with experiment, it would be useful to consider this in terms of pressure. n_e, the electron density, is proportional to the pressure, and v_d, the drift velocity, is proportional to the root of the electric field and thus the root of the charge. This can be seen by taking the kinematic equation $v_f^2 = 2ad$ and plugging in the acceleration to get $v_f = \sqrt{\frac{2eEd}{m_e}} = \sqrt{\frac{2ek_eQd}{m_e r^2}} \sim \sqrt{Q}$. Although the simulations do include electron scattering, because of the low densities involved we do not assume that the drift velocity is proportional to the electric field as one might infer from the Drude model. Instead we assume that the electrons flow freely towards the charged target with negligible scattering. These considerations reduce the equation to:

$$\frac{dQ}{dt} = P * C * \sqrt{Q} \tag{2}$$

where

$$C = \frac{eA}{RT} * \sqrt{\frac{2ek_e d}{m_e r^2}} \tag{3}$$

R is the ideal gas constant, T is temperature, k_e is the Coulomb constant, and d is the distance traveled by the particles. This differential equation is then solved using separation of variables to derive an expression for the charge in terms of time.

$$\frac{dQ}{\sqrt{Q}} = P * C * dt \tag{4}$$

$$\sqrt{Q(t)} - \sqrt{Q_0} = \frac{P * C * t}{2} \tag{5}$$

$$Q(t) = (\sqrt{Q_0} - \frac{P * C * t}{2})^2 \tag{6}$$

This above derived expression for $Q(t)$ is then plugged into the equation for the voltage:

$$V(t) = \frac{k_e Q}{r} \tag{7}$$

$$V(t) = k_e \frac{(\sqrt{Q_0} - \frac{P*C*t}{2})^2}{r} \tag{8}$$

From there, multiplying the voltage by the electron charge gives the minimum kinetic energy needed for an electron to escape the target's electric field. We assume electrons in the target follow an exponential distribution in energy that is characterized by a "hot" temperature, T_h. By integrating this electron distribution from the minimum energy to infinity, the total number and total kinetic energy of the escaping particles is calculated. This Maxwell-Boltzmann distribution is approximated to an exponential distribution based on the Boltzmann factor $e^{-E/kT}$. In the following equations, this approximate distribution is integrated over the range of electrons that can escape to determine the mean energy of escaping electrons. Multiplying this by the number of escaping electrons gives the total energy of accelerated electrons.

$$\text{TotalEnergy} = \frac{q_{esc}}{e} < KE >= \int_{eV(t)}^{\infty} \frac{n_0}{e} * KE * e^{\frac{-KE}{k_b T_h}} dKE \tag{9}$$

$$\text{TotalEnergy} = \frac{q_{esc}}{e} < KE >= \frac{n_0}{e} k_b T_h e^{\frac{eV(t)}{k_b T_h}} (eV(t) + k_b T_h) \tag{10}$$

where n_0 is a normalization constant. The laser-to-electron conversion efficiency is the E_{total}/E_{laser}, which means that the calculated energy $\frac{q_{esc}}{e} < KE >$ is proportional to the conversion efficiency for the same pulse energy.

However, for the Maxwell-Boltzmann distribution, the distribution is proportional to $Ee^{-E/kT}$. By applying the same mean calculation, the following result for the total energy of the electrons is derived.

$$\text{TotalEnergy} = \frac{q_{esc}}{e} < KE >= \frac{n_0}{e} k_b T_h e^{\frac{-eV}{k_b T_h}} ((eV)^2 - 2 * k_b T_h eV + 2(k_b T_h)^2) \tag{11}$$

Equation 10 and 11 gives a total energy for the electrons, as given by each distribution, that can be compared against the simulation results to determine which distribution matches best.

3 Methods

For this project, the interaction of the laser pulse with the target was simulated under a range of background pressures in LSP, a particle-in-cell (PIC) simulation software, to gain insight into how the background pressure is affecting the electrons. The particle-in-cell method models the system as particles and can best illustrate how the electrons are reacting to the pulse. A better understanding of this effect could facilitate the design of future experiments in improving laser-to-electron conversion efficiency and may provide insight into how the background pressure is affecting ion acceleration on longer timescales.

3.1 Particle-in-Cell Codes

In order to best simulate the effect of the background pressure on the laser-target system, we used the particle-in-cell (PIC) method. Particle-in-cell simulates the system using macroparticles, which are computational constructs that represent many physical particles and are used to reduce the number of calculations necessary. This approximation is crucial especially for modeling a near solid density targets as we are doing here. Simulating all of the physical particles present would require simulating an Avogadro's number of particles (10^{23}). This poses two massive problems for current machines: processing speed and memory. Processors, in the best case scenario, can only perform 10^{10} computations per second; computing even one time step is impossible in any reasonable amount of time. Additionally, for every particle, we must store the particles' positions and momenta; that is five floating point values for a 2D3V simulation. This is a memory requirement of at least 10^{23} bytes, which is also not feasible with today's machines. The macroparticle approximation solves these issues by reducing the number of particles from a daunting 10^{23} to a more manageable 10^6 - 10^8. Importantly, the charge-to-mass ratio of these macroparticles is the same as microscopic particles that they represent, which means they will respond to electric and magnetic fields very much as a group of the particles they represent would.

PIC codes also discretize quantities such as the fields by mapping the simulation space to a grid of cells. For every time step, the PIC simulation first takes the initial particle positions and velocities and uses them to calculate the charge density and current density at every grid point. The code then solves Maxwell's equations for the electric and magnetic field at the grid points using these charge and current densities. The electric and magnetic fields at every particle position are approximated by interpolation. The force for every particle is calculated from the electric and magnetic fields using the Lorentz Force equation. Using kinematics, PIC calculates the particle positions and velocities for the

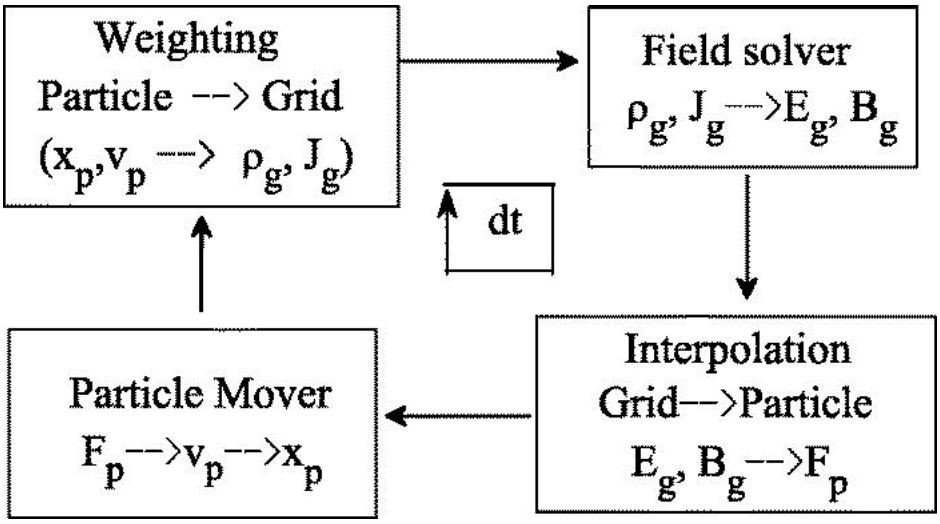

Figure 5: Overview of the Particle-in-Cell computational cycle for a single time step. The particle positions and velocities are used to calculate the electric and magnetic fields at grid points. Through interpolation, the fields are used to calculate the force and thus the motion of each particle. [7]

next time step. This cycle is repeated for every time step; Figure 5 shows an overview of this cycle.

3.2 Simulation Details

LSP was the specific PIC program used for these simulations. LSP is commonly used to study laser-particle interactions. One important reason for this is that LSP goes further than the PIC code described above through handling collisions between particles rather than the particles solely interacting through the fields. Additionally, LSP offers a high level of customization in both the initialization and evolution of the simulation.

The LSP simulation code was executed in 2D3V, meaning two-dimensional space and three-dimensional velocity. This was done to reduce computational time. A three-dimensional simulation would necessarily increase the number of macroparticles and the number of computations needed and drastically lengthen the computational time. A typical two-dimensional simulation on RAMSES-II took approximately 24 hours to finish whereas a three-dimensional simulation would likely take weeks. Twelve of these two-dimensional simulations were performed, each modeling the interaction with a

different background pressure ranging from 8 mTorr to 300 Torr (atmospheric pressure) to map the behavior with increasing pressure. Each simulations had a duration of 350 femtoseconds with a time step of 0.1 fs, and the simulation starts with four species: singly ionized carbon atoms, singly ionized oxygen atoms, protons, and electrons, which simulate the elemental composition of ethylene glycol. The pre-pulse, a weaker secondary pulse that precedes the main pulse, is assumed to have singly ionized the entire target including the surrounding background plasma due to its intensity.

Within the simulation itself, the target was simulated as a block of near solid density ethylene glycol approximately ten microns thick and a pre-plasma with an exponential fall-off extended in front of it. Ethylene glycol is the current target liquid in our experiment and in our simulation as its low vapor pressure allows it to remain liquid closer to vacuum. Additionally, the pre-plasma represents a cloud of ionized gas ejected from the target by the pre-pulse. A very low density ethylene glycol plasma was placed around the target to simulate the ambient plasma applying the background pressure on the target. Ethylene glycol is the current target liquid in our experiment and in our simulation as its low vapor pressure allows it to remain liquid closer to vacuum. In addition, a laser pulse was also simulated with an intensity of 10^{18} W/cm^2, a duration of 42 fs, and a wavelength of 800 nm; these parameters match that of the Red Dragon laser, a Ti:Sapphire laser system, at AFRL.

The simulations were each executed on a node of Ohio State's High Energy Density Physics (HEDP) group's dedicated cluster, RAMSES-II, as well as on the ERDC's supercomputer Onyx. RAMSES-II consists of 6 nodes. Each node has 300 GB of local storage space, 130 GB of RAM, and 48 cores. The HEDP group also had existing Python tools for reading and plotting the simulation results, and these were used for analyzing the LSP output files.

4 Results

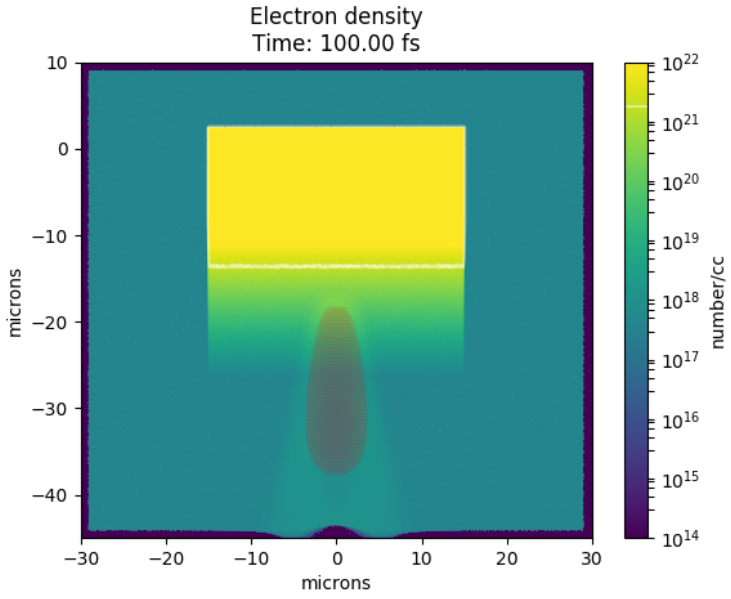

(a) Visualization of the Simulation Electrons

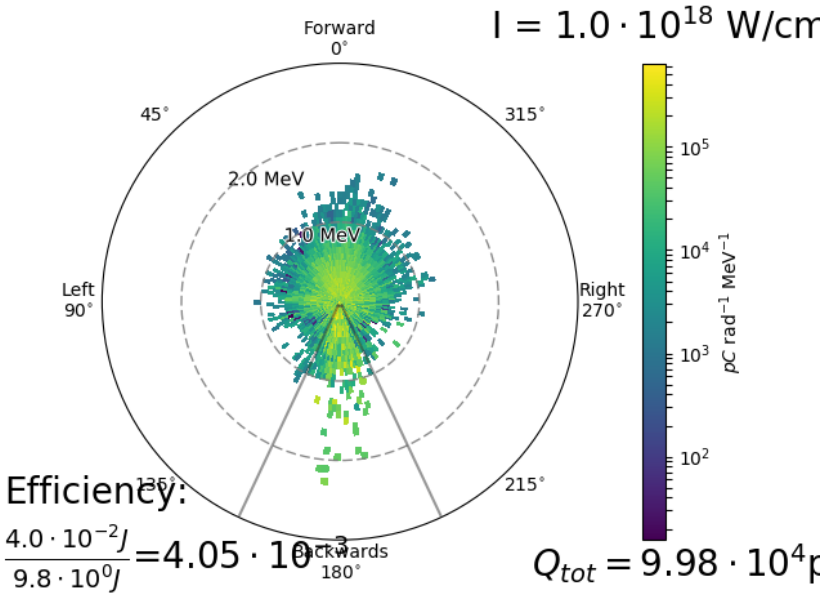

(b) Electron Energy Polar Histogram

Figure 6: Output plots for the simulations. (a) Visualization of the simulation showing the target with the pre-plasma in front. The laser pulse is shown in red propagating from the bottom. (b) Example of a plot of the results. 2D polar histogram of the escaping electrons showing energy and angle of motion.

The simulations provided output files with the particle position at each timestep for a given

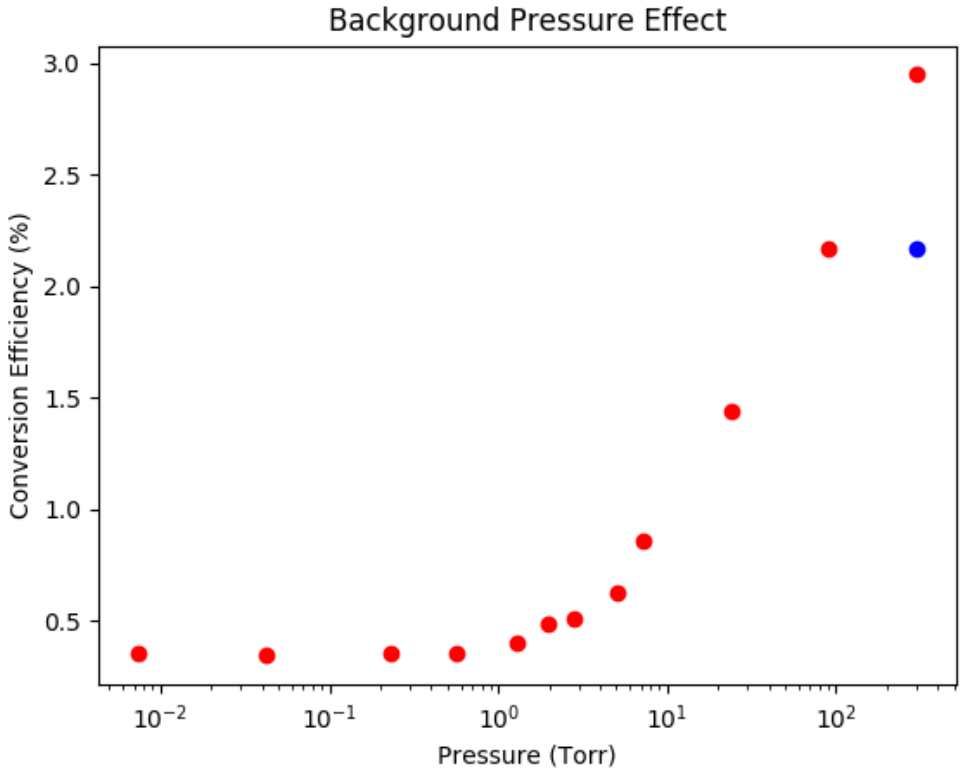

Figure 7: Semi-log plot of the background pressure vs. laser-to-electron conversion efficiency for the twelve different ambient pressures. The laser-to-electron conversion efficiency is calculated from the total energy of the backwards-accelerated electrons. In the 300 Torr case, some of the accelerated electrons came from the background plasma. The blue data point represents the efficiency taking into account only electrons from the target.

species in order to visualize the simulation. In this case, electrons were visualized as in Figure 6a. The simulations also collected the information of the escaping particles including the initial position, the energy, and the angle of each particle. This information can be used to produce energy spectra such as the Figure 6b, which gives both the energy and angle. A laser-to-electron conversion efficiency, which is the ratio of the energy of the accelerated electrons to the pulse energy, was calculated for the back-scattered electrons with energies greater than 100 keV because these are the electrons that escape and are detected. Back-scattered was defined as electrons moving within 22.5 degrees opposite the laser propagation direction. The results of the batch of twelve simulations were plotted in Figure 7 (though the 90 and 300 Torr cases had a pulse energy of 10.2 J as opposed to 9.8 J set in the

simulation with negligible differences in intensity). The 300 Torr case was adjusted down from 3.07% to 2.17% with a correction factor because a significant portion (26%) of the escaping electrons came from the background plasma, and this is noted accordingly in the plot. The conversion efficiency appears to remain flat with little change until the pressure increases to the order of one Torr. After one Torr, the efficiency grows exponentially with the pressure. Finally, the efficiency reaches a plateau around 90 Torr.

5 Discussion

As can be seen from the results, the background pressure is clearly having a drastic effect on the laser-to-electron conversion efficiency, and it is playing a significant role in facilitating electron acceleration from the target. Two analytic models have been developed based on the resistor-capacitor model.

$$\text{TotalEnergy} = \frac{q_{esc}}{e} < KE >= \frac{n_0}{e} k_b T_h e^{\frac{eV(t)}{k_b T_h}} (eV(t) + k_b T_h) \tag{12}$$

$$\text{TotalEnergy} = \frac{q_{esc}}{e} < KE >= \frac{n_0}{e} k_b T_h e^{\frac{-eV}{k_b T_h}} ((eV)^2 - 2 * k_b T_h eV + 2(k_b T_h)^2) \tag{13}$$

These models were derived by calculating the potential wall, which the escaping electrons experience over time given a stream of free-flowing electrons moving into the target to neutralize it. This potential was then used to calculate the average energy of the escaping electrons assuming an exponential distribution and then again assuming a three-dimensional Maxwell-Boltzmann distribution.

From the equations 10 and 11 derived previously, which were derived previously, both models were rendered over the range of energies from 10 mTorr (near vacuum) to 300 Torr (near atmospheric pressure) as shown in Figure 8 using reasonable assumptions for the parameters. The data in Morrison *et al* has the escaping charge in the hundreds of picoCoulombs and the pulse energy in the millijoules.

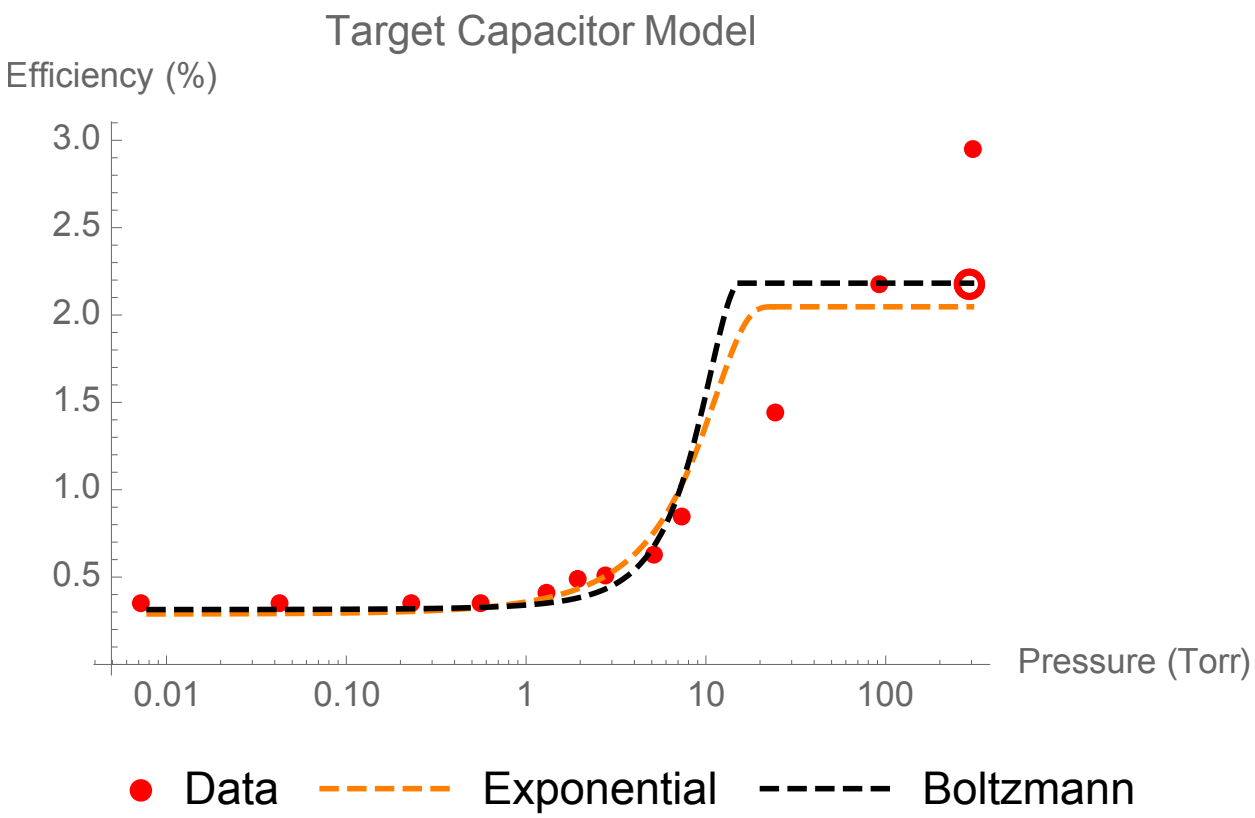

Figure 8: Comparison of the two analytic models for this hypothesis by using approximate parameters such as a pulse energy of 3 mJ and by calculating the energy of escaping electrons[4]. "Exponential" shows the analytic model assuming a simple exponential distribution for the energy of the electrons. "Boltzmann" shows the analytic model assuming a Maxwell-Boltzmann distribution for the electron energies. The red empty data point represents the adjustment accounting for background electrons. The 300 Torr case was not included in the fitting because of this.

[4] The scale for motion r and d on this time scale is on the order of microns, so the length scale was bounded near 5 microns. The time scale used was the pulse duration of 42 fs. The conversion efficiency is simply the electron energy divided by the pulse energy. By using an approximate pulse energy of 3 mJ based on the experiment and considering that 15% of the escaping electrons scattered backward based on the simulation, both models can be converted from energy to conversion efficiency and compared directly with the simulation results. For both models, kT_h, the charge Q_0, and the length scale r were varied to find the best fit. The Boltzmann plot in Figure 8 approximately matches the results including the transition around 10 Torr and a plateau in the tens of Torr. This fit requires

an initial charge of 480 pC, a hot temperature energy kT_h of 450 keV, and a length scale of 6.9 microns. On the other hand, the Exponential fit in Figure 8 also somewhat matches the results, although it transitions at a lower pressure than the results, and has a plateau around the same range as the Boltzmann plot. However, this fit is based on a Q_0 of 1.01 nC and a kT_h of approximately 400 keV, and a length scale of 6.58 microns. Both distributions match within an order of magnitude the results of the simulation with realistic parameters. Of the two distributions, assuming an exponential distribution matches the results slightly better than assuming a Boltzmann distribution, in particular, the gentler slope of the transition on the Exponential plot. Furthermore, while both initial charges are plausible, 1 nC and a lower kT_h are somewhat more realistic. The notable observation, however, is that the transition occurs around the same pressure range as in the simulations.

5.1 Future Work

In these simulations, the effect on the ion acceleration could not be captured due to the long timescales required. Ions, being much more massive than electrons, require much longer timescales on the order of picoseconds to be accelerated whereas the simulation only lasted 350 femtoseconds. However, the electron dynamics observed here on shorter timescales, due to the role of electrons in TNSA, are key to understanding the ion dynamics on longer timescales. That said, simulations to capture the ion acceleration may be a possible future avenue to provide more concrete look into the ion dynamics. This will be challenging as it will require larger simulations with much longer simulation (ps) and longer wall times (weeks).

In addition, three-dimensional simulations are being developed to better model the electron acceleration. While two-dimensional simulations can provide good insight into the physical behavior of these systems, it can fail to depict the full picture. A three-dimensional simulation is closer to

the physical reality. This is challenging as it will require larger simulations and three-dimensional simulations are difficult to write compared to its two-dimensional counterpart.

In conclusion, we have simulated the electron dynamics at the hundreds of femtoseconds timescale and mapped out the relationship between the conversion efficiency and background pressure with twelve data points. The analytic model of our hypothesis has been developed to compare with these results and has shown good agreement with them for realistic parameters. Electrons are only one piece of the puzzle, however. We aim to both refine our understanding of the electron dynamics by moving to three-dimensional simulations and to capture the ion dynamics in our simulations.

6 Acknowledgements

This research is supported by the Air Force Office of Scientific Research under LRIR Project 17RQ-COR504 under the management of Dr. Riq Parra and Dr. Jean-Luc Cambier. Support was also provided by the DOD HPCMP Internship Program and the University of Dayton Research Institute.

References

[1] J. T. Morrison, S. Feister, K. D. Frische, D. R. Austin, G. K. Ngirmang, N. R. Murphy, C. Orban, E. A. Chowdhury, and W. M. Roquemore. MeV proton acceleration at kHz repetition rate from ultra-intense laser liquid interaction. *New Journal of Physics*, 20(2):022001, February 2018.

[2] M. Passoni, L. Bertagna, and A. Zani. Target normal sheath acceleration: theory, comparison with experiments and future perspectives. *New Journal of Physics*, 12(4):045012, April 2010.

[3] S. Feister, D. R. Austin, J. T. Morrison, K. D. Frische, C. Orban, G. Ngirmang, A. Handler, J. R. H. Smith, M. Schillaci, J. A. LaVerne, E. A. Chowdhury, R. R. Freeman, and W. M. Roquemore. Relativistic electron acceleration by mJ-class kHz lasers normally incident on liquid targets. *Optics Express*, 25:18736, August 2017.

[4] J. T. Morrison, E. A. Chowdhury, K. D. Frische, S. Feister, V. M. Ovchinnikov, J. A. Nees, C. Orban, R. R. Freeman, and W. M. Roquemore. Backward-propagating MeV electrons from 10^{18} W/cm^2 laser interactions with water. *Physics of Plasmas*, 22(4):043101, April 2015.

[5] H. Schwoerer, S. Pfotenhauer, O. Jäckel, K.-U. Amthor, B. Liesfeld, W. Ziegler, R. Sauerbrey, K. W. D. Ledingham, and T. Esirkepov. Laser plasma acceleration of quasi-monoenergetic protons from microstructured targets. *Nature*, 439:445–448, January 2006.

[6] A. Link, R. R. Freeman, D. W. Schumacher, and L. D. van Woerkom. Effects of target charging and ion emission on the energy spectrum of emitted electrons. *Physics of Plasmas*, 18(5):053107, May 2011.

[7] X. Qi, Y.-x. Xu, W.-s. Duan, L.-y. Zhang, and L. Yang. Particle-in-cell simulation of the head-on collision between two ion acoustic solitary waves in plasmas. *Physics of Plasmas*, 21(8):082118, August 2014.

7 Appendix

7.1 All Output Polar Histograms

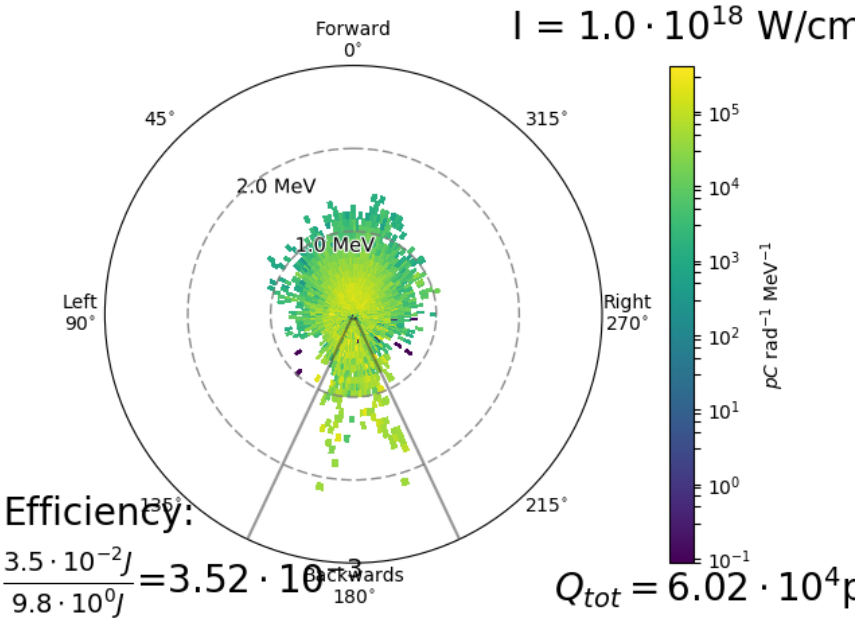

Figure 9: 7.8 mTorr

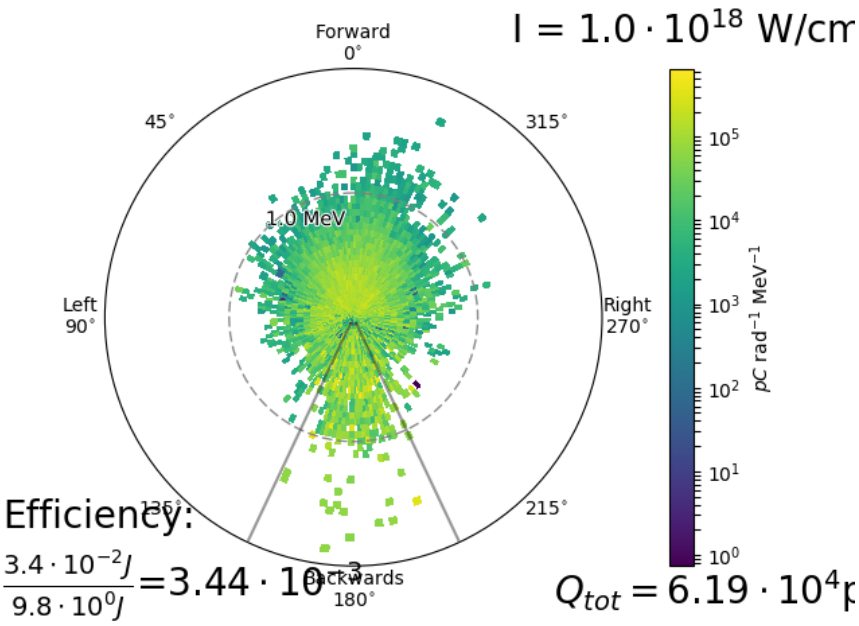

Figure 10: 45.5 mTorr

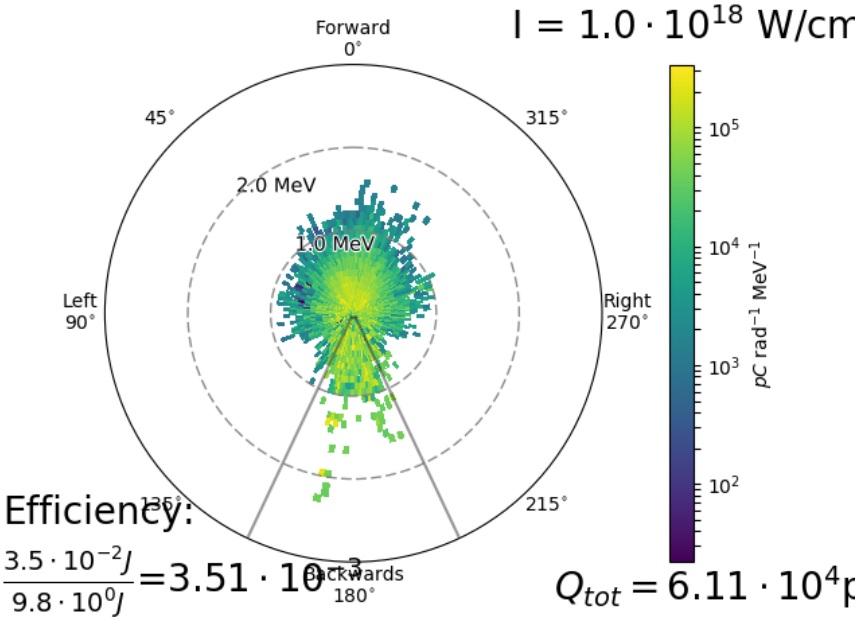

Figure 11: 248.8 mTorr

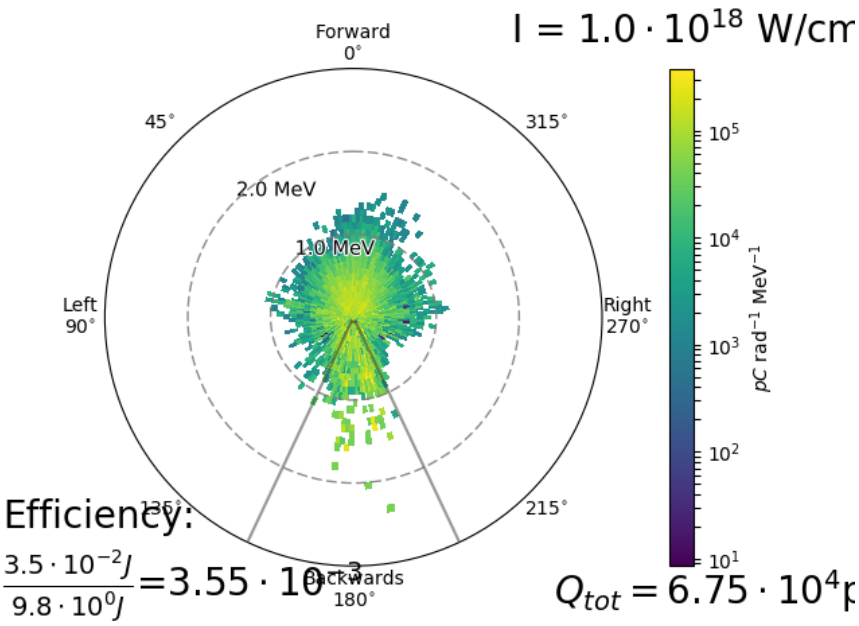

Figure 12: 0.607 Torr

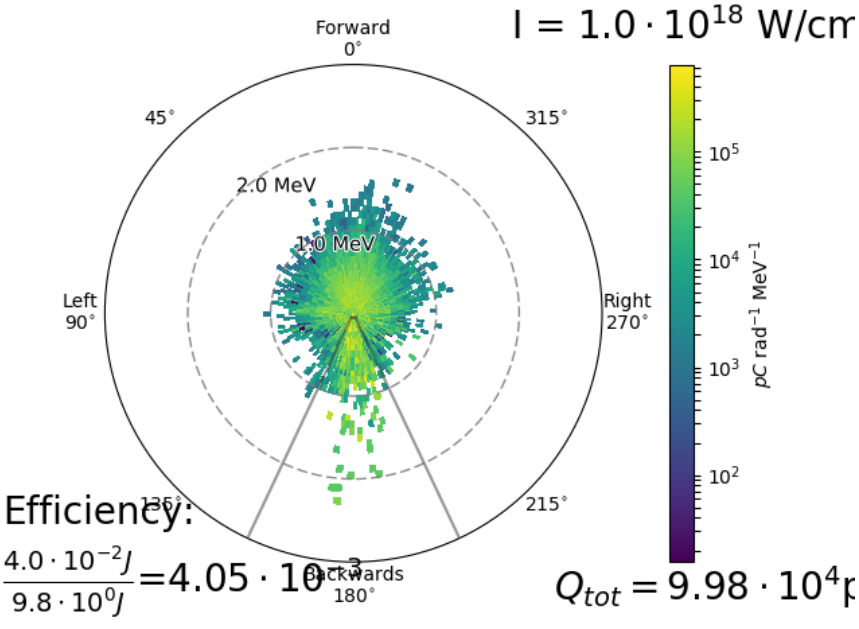

Figure 13: 1.360 Torr

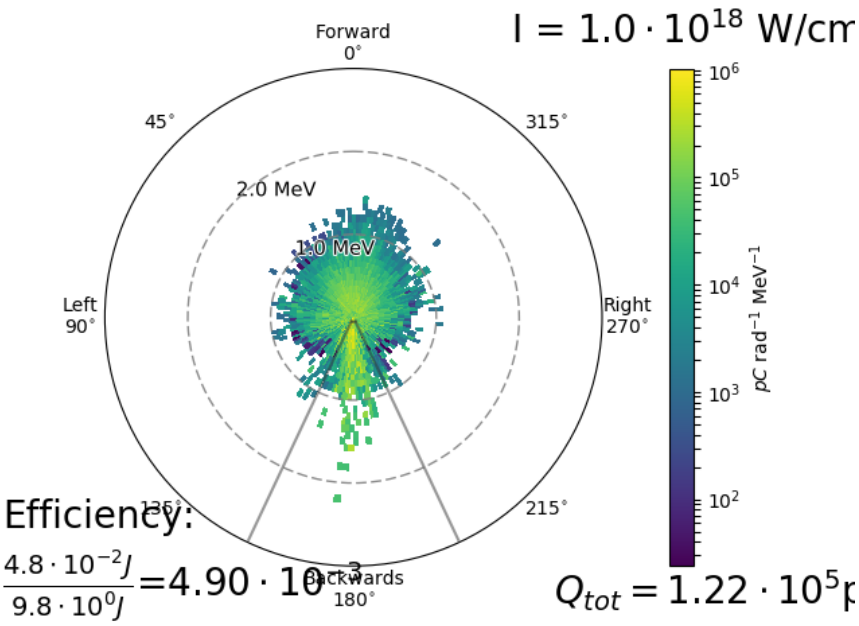

Figure 14: 2.124 Torr

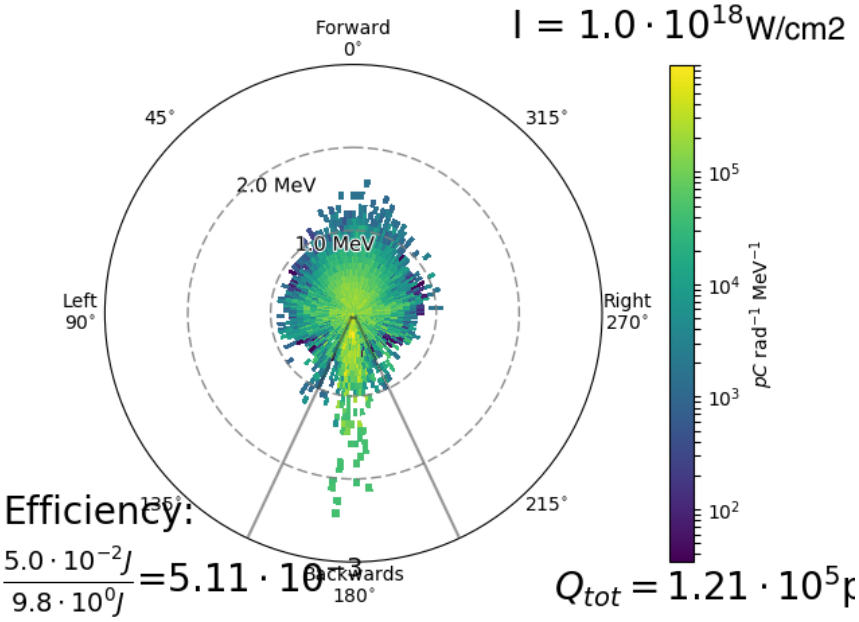

Figure 15: 3.035 Torr

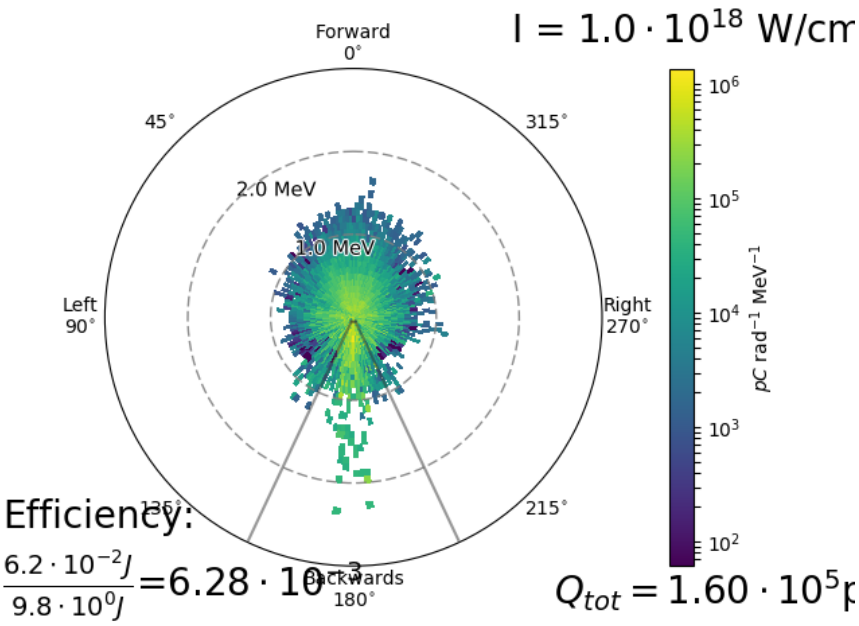

Figure 16: 5.462 Torr

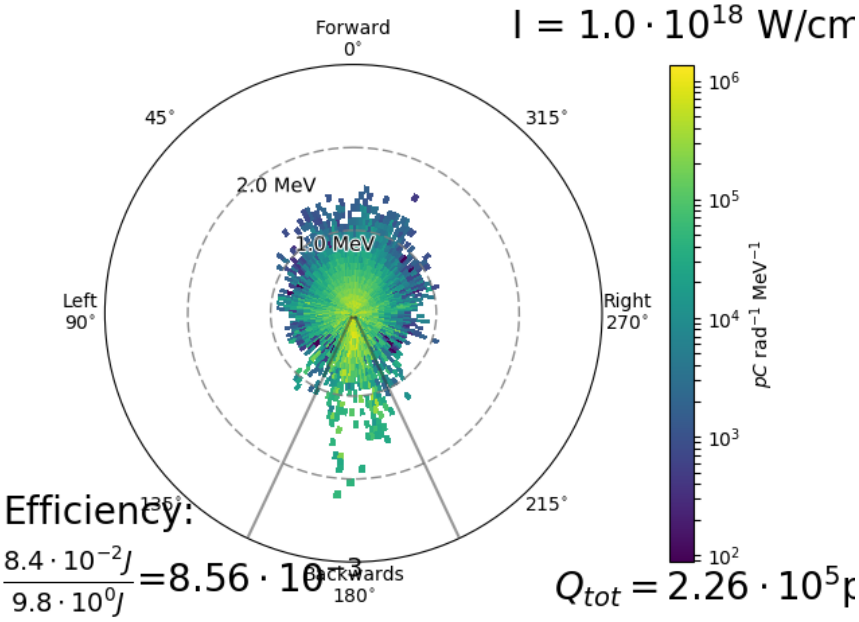

Figure 17: 7.890 Torr

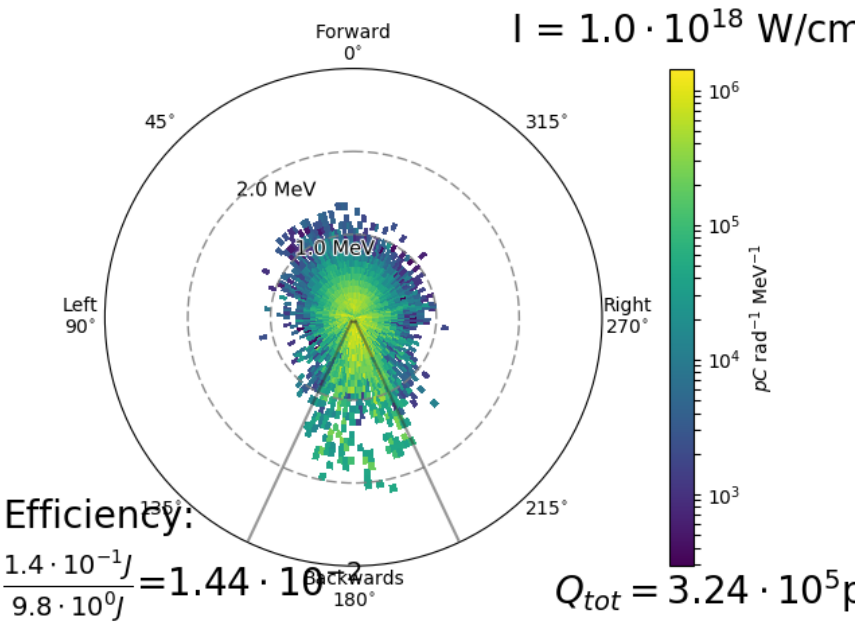

Figure 18: 26.1 Torr

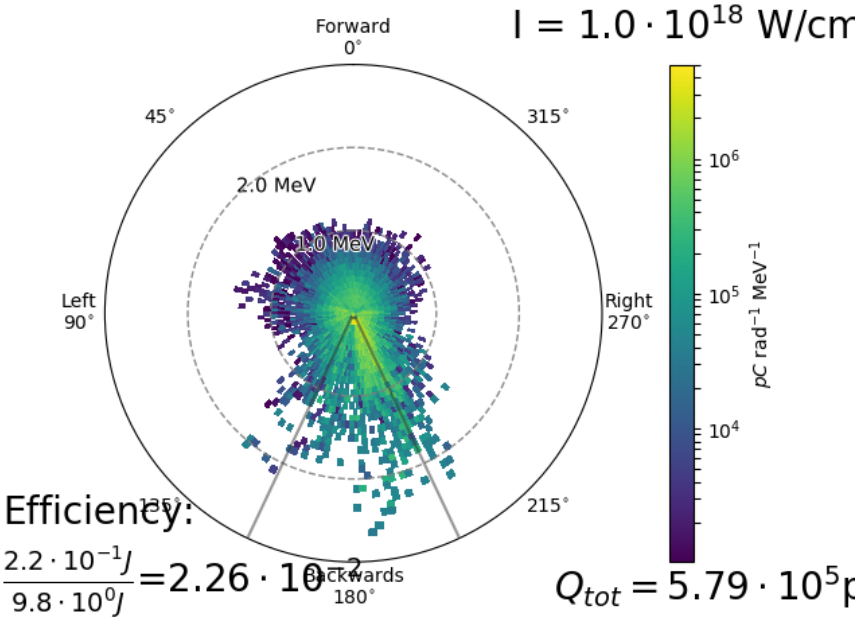

Figure 19: 91.04 Torr

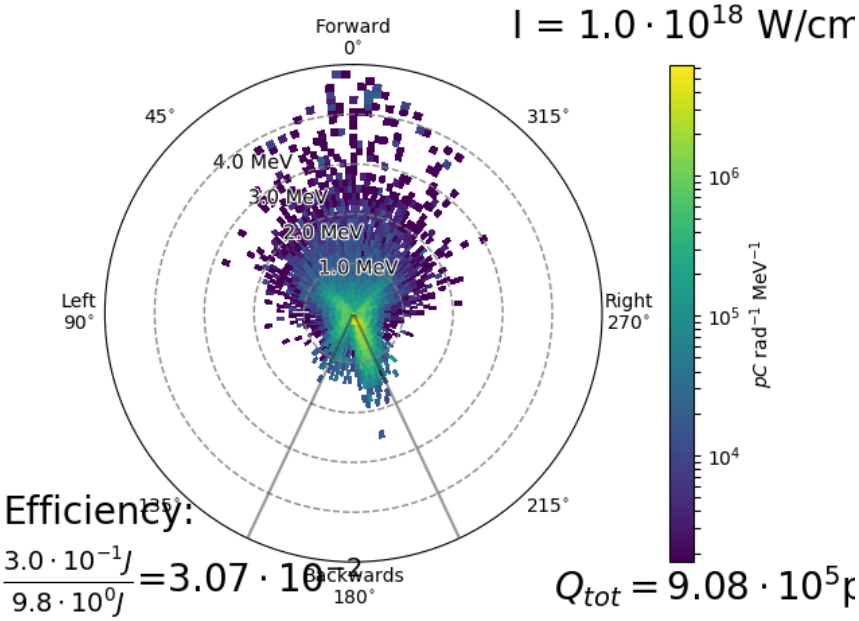

Figure 20: 303.46 Torr